*Korean J. Chem. Eng.*, 33(3), 934-944 (2016)
DOI: 10.1007/s11814-015-0224-6

pISSN: 0256-1115
eISSN: 1975-7220

# Size-controlled synthesis of chalcogen and chalcogenide nanoparticles using protic ionic liquids with imidazolium cation

**Boominathan Meenatchi*,†, Velayutham Renuga**, and Ayyar Manikandan*****

*Department of Chemistry, Cauvery College for Women, Trichy, Tamilnadu, India
**Department of Chemistry, National College, Trichy, Tamilnadu, India
***Department of Chemistry, Bharath Institute of Higher Education and Research, Bharath University, Chennai - 600 073, Tamilnadu, India
(*Received 16 July 2015 • accepted 22 October 2015*)

**Abstract**−Green synthesis of selenium (chalcogen) nanoparticles (SeNPs) has been successfully attained by simple wet chemical method that involves the reaction of six different protic ionic liquids with imidazolium cations and sodium hydrogen selenide (NaHSe) in the presence of poly ethylene glycol-600 (PEG-600) as an additional stabilizer. The obtained SeNPs were characterized using UV spectral (UV), Fourier transform infra-red (FT-IR), X-ray diffraction (XRD), thermogravimetric analysis (TGA), differential thermal analysis (DTA), scanning electron microscope (SEM) with energy dispersive X-ray (EDX) and high resolution transmission electron microscope (TEM) analysis. The results illustrate that the synthesized SeNPs are spherical in shape with size ranging 19-24 nm and possess good optical property with greater band gap energy, high thermal stability up to 330 °C, low melting point of 218-220 °C comparing to precursor selenium. Using the synthesized SeNPs, two chalcogenides such as ZnSe and CdSe semiconductor nanoparticles were synthesized and characterized using XRD, SEM with EDX and TEM analysis. The fabricated CdSe and ZnSe nanoparticles appeared like pebble and cluster structure with particle size of 29.97 nm and 22.73 nm respectively.

Keywords: Protic Ionic Liquids, Selenium Nanoparticles, Semiconductor, Chalcogenides, Optical Property

## INTRODUCTION

Nanoparticle synthesis employing ionic liquids (ILs) has garnered new attention in the field of green chemistry, especially, ILs with imidazolium cation [1]. Ionic liquids are fluids composed of organic cation and inorganic or organic anion [2]. ILs can be known as 'designer solvents' because of their chemical and physical properties like melting point, viscosity, density, hydrophobicity and polarity shall be modified by altering the nature of their cations and anions [3]. ILs are normally stable in air and water and have low melting points [4]. They can be used as green solvents and stabilizers for nanoparticle synthesis due to their general ease of synthesis, stability (nonflammable, thermally stable), and low vapor pressure [5,6]. Ionic liquids with the general characteristics of low interfacial tension permit in adapting to the surrounding reaction media, and their relative solubility can be tuned by varying their anionic and cationic components [5]. Many nanostructured materials are synthesized by using ionic liquids as precursors [8-10]. Ionic liquids with imidazolium cation comprise pre-organized structures via hydrogen bonds that bring structural directionality [11,12]. They tend to act as a potential key for the preparation of nanostructures due to their exclusive combination of adaptability towards various molecules and phases.

Pure selenium along with selenium containing nanomaterials has admirable photoelectrical characteristics, semiconductor properties and high biological activity [13]. Nano-selenium has large piezoelectric, high photoconductivity, thermoelectric and non-linear responses and is used in photocells, photographic exposure meters, xerography, electrical rectifiers etc., [14]. In addition, red selenium nanoparticles have excellent biological activity and low toxicity [15]. The nanowires of trigonal selenium have novel photoconductivity [16]. The amorphous selenium nanoparticles contain unique photoelectric, semiconducting and x-ray-sensing properties [17]. It possess high reactivity and leads to a variety of functional materials like $Ag_2Se$ [18], CdSe [18], ZnSe [19] and PbSe [19]. Hence, the selenium nanoparticle has a scope of research. The conventional synthesis of SeNps is concerned in the use of toxic reagents and expensive instruments and also associated with certain complicated post-treatment process. Due to the higher advantages of ionic liquids, the synthesis of SeNPs in controlled size and morphology is attained by a new class of ionic liquids known as protic ionic liquids (PILs) formed by the variety of proton transfer from Brönsted acids to Brönsted base with imidazolium cation [20].

This paper imparts a new path for the synthesis of SeNPs by the reaction of sodium hydrogen selenide with each of six PILs 2-methylimidazolium lactate ([Hmim]$CH_3CH(OH)COO^-$), 1-ethylimidazolium lactate ([Heim]$CH_3CH(OH)COO^-$), 1-butylimidazolium lactate ([Hbim] $CH_3CH(OH)COO^-$), 2-methylimidazolium glycolate ([Hmim]$CH_2(OH)COO^-$), 1-ethylimidazolium glycolate ([Heim] $CH_2(OH)COO^-$), 1-butylimidazolium glycolate ([Hbim] $CH_2(OH)COO^-$) individually in the presence of PEG-600 as an

†To whom correspondence should be addressed.
E-mail: meenachemist@gmail.com

additional stabilizer. NaHSe was obtained by the reaction of selenium with $NaBH_4$. By using one of the synthesized SeNPs as precursor, ZnSe and CdSe nanoparticles were synthesized. The ZnSe and CdSe are found to be useful semiconductors with a wide optical band gap.

## EXPERIMENTAL

### 1. Materials

2-Methylimidazole, 1-ethylimidazole, 1-butylimidazole, lactic acid, glycolic acid, selenium powder, sodium borohydride, polyethylene glycol-600 (PEG-600) were purchased from Sigma-Aldrich and utilized exclusive of further purification. Cadmium sulfate and zinc acetate with AR quality were also purchased.

### 2. Synthesis of Imidazolium Protic Ionic Liquids

An equimolar ratio of the precursor Brönsted acids (hydroxy carboxylic acids) and Brönsted bases (substituted imidazoles) were taken in a reaction vessel and stirred with a magnetic stirrer for an hour, later subjected to microwave irradiation for a determined period of time and power level [21]. The protic ionic liquids were formed according to Scheme 1.

### 3. Preparation of Sodium Hydrogen Selenide (NaHSe)

A mixture of 1 gm of selenium powder, 3 gm of $NaBH_4$ and 15 ml of deionized water in a reaction vessel was stirred well and heated to 40 °C for an hour. The resulting homogeneous solution of sodium hydrogen selenide (NaHSe) was washed with excessive water.

$$4\,NaBH_4+2Se+7\,H_2O\rightarrow 2NaHSe+Na_2B_4O_7+14\,H_2 \quad (1)$$

### 4. Synthesis of SeNPs

The aqueous solution of sodium hydrogen selenide and 1 ml of PEG-600 was added with 5 ml of [2 mim] $CH_3CH(OH)COO^-$. For nearly 6 hours the reaction mixture was stirred at 80 °C with a magnetic stirrer, later cooled and kept at room temperature (27 °C) for 24 hrs. Using centrifugation, the SeNPs deposited in the bottom of the reaction vessel were recovered.

The above-mentioned process was carried out for the leftover PILs like [Heim]$CH_3CH(OH)COO^-$, [Hbim]$CH_3CH(OH)COO^-$, [Hmim]$CH_2(OH)COO^-$, [Heim]$CH_2(OH)COO^-$, [Hbim] $CH_2(OH)COO^-$ separately in different reaction vessels.

### 5. Preparation of CdSe Nanoparticles

0.2 g of $CdSO_4$ in 10 ml of deionized water was added to the

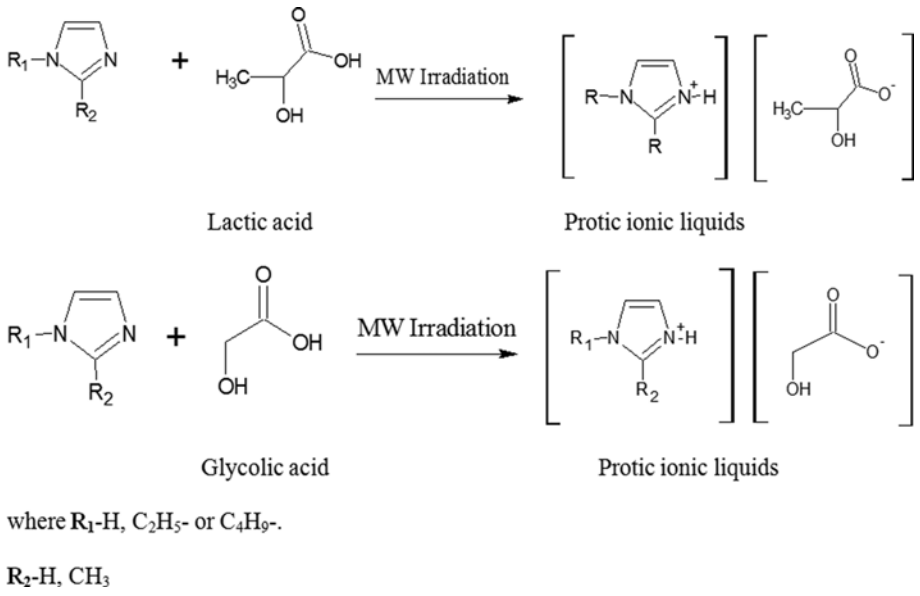


**Scheme 1. Schematic diagram of synthesis of protic ionic liquids.**

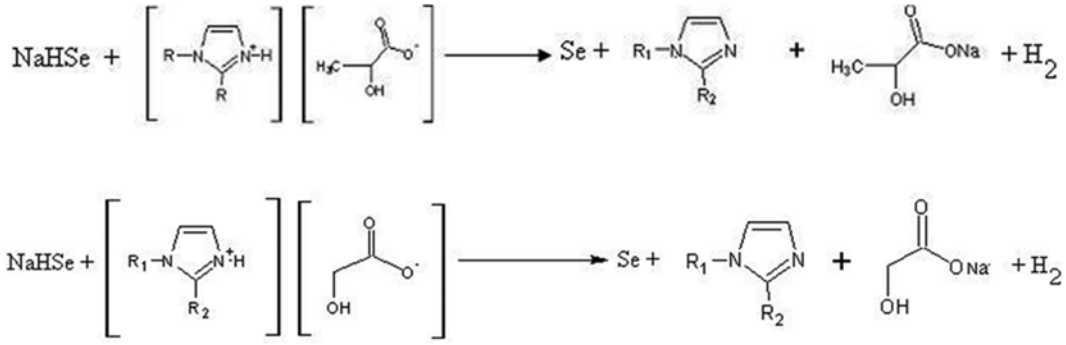


**Scheme 2. Schematic diagram of synthesis of selenium nanoparticles.**

solution of 0.2 g of SeNPs (synthesized using [Hbim] $CH_2(OH)COO^-$ which stabilized the SeNPs to a larger extend than the rest of the PILs) in 2 ml [Hbim] $CH_2(OH)COO^-$ and 1 ml of PEG-600. The obtained mixture was stirred for 6 hours with a magnetic stirrer at 60 °C. The black precipitate of CdSe was extracted and washed with ethanol and hot distilled water several times.

**6. Preparation of ZnSe Nanoparticles**

The mixture of zinc acetate (0.2 g), 10 ml of deionized water and 0.2 g of SeNPs (synthesized using [Hbim] $CH_2(OH)COO^-$) was stirred well for 3 hrs and later heated to 120 °C for 2 hrs. The black precipitate of ZnSe was extracted and washed quite a few times with acetone and hot distilled water.

**7. Characterization Techniques**

The absorption spectrum was recorded by Perkin Elmer Lambda35 Spectrometer and the energy band gap was calculated using the direct formula [21] $E_g^o$ (eV)=12397.8/$\lambda_{max}$ (Å), where $E_g^o$ is the energy band gap and $\lambda_{max}$ is the wavelength at which the maximum absorption is shown. The FT-IR spectra were recorded using the Jasco (FT-IR 460) spectrometer. The XRD measurement was carried out by XPERT-PRO diffractometer which utilizes Cu-K$\alpha$ (1.5406 Å). SEM and TEM images were obtained using VEGA3-TESCAN Jeol/JEM 2100 instrument. The TGA and DTA measurements were performed using Perkin Elmer/TGA4000 analyzer.

## RESULTS AND DISCUSSION

**1. Selenium Nanoparticles (SeNPs) and CdSe, ZnSe Nanoparticles**

All the synthesized protic ionic liquids were acidic [21]. Sodium hydrogen selenide was decomposed in the ionic liquids (acidic medium) in the presence of PEG-600 to yield SeNPs as shown in Eq. (2). The course of reaction involved in the transfer of proton from PILs and reacted with NaHSe to produce elemental SeNPs is shown in Scheme 2. Subsequently, these nanoparticles were coated by the [Hbim] $CH_2(OH)COO^-$ ionic liquid, and this coating impeded further growth of the particles. Furthermore, the low interfacial tension of ionic liquids led to high nucleation rates and enabled the generation of small nanoparticles [22]. Additionally, the high viscosity of surrounding medium (ionic liquids with $\eta$ = 1216 cP) minimized the probability of close contact of nanoparticles, thereby inhibiting the growth of particles that results in smaller selenium nanoparticles.

The PIL ([Hbim] $CH_2(OH)COO^-$) acted not only as a reducing agent but also as a stabilizer in the formation of CdSe and ZnSe nanoparticles. The first step in both the cases was involved in the reduction of elemental SeNPs to $Se^{2-}$ ions by [Hbim] $CH_2(OH)COO^-$. The generated selenide ions react with $Cd^{2+}$ (from Cadmium sulphate) and $Zn^{2+}$ (from Zinc acetate) resulting CdSe and ZnSe, respectively, with a higher yield (Scheme 3 and Scheme 4).

Later, the resulting CdSe and ZnSe nanoparticles were electrostatically stabilized using [Hbim] $CH_2(OH)COO^-$. The $[Hbim]^+$ cations of [Hbim] $CH_2(OH)COO^-$ combined together with selenide moieties of CdSe and ZnSe through electrostatic attraction and formed a layer around the nanoparticles. As a result, the surrounding layer formed by $[Hbim]^+$ hindered the agglomeration of the obtained CdSe and ZnSe nanoparticles in the solution, resulting in smaller particles. In the absence of PIL, small CdSe and ZnSe nanoparticles grow and form CdSe and ZnSe aggregates, respectively, with a larger size. Hence, the rate for nucleation of nanoparticles prepared in presence of the PIL is higher than the prepared sample in other aqueous solutions.

**2. UV-spectral Studies**

The strong absorption bands with absorption maximum 262.9, 223.9, 217.9, 259.47, 221.8, 213.69 nm with transmittance ranging from 0.2740 to 0.5269 were observed for SeNPs obtained from [Hmim]$CH_3CH(OH)COO^-$, [Heim]$CH_3CH(OH)COO^-$, [Hbim] $CH_3CH(OH)COO^-$, [Hmim]$CH_2(OH)COO^-$, [Heim] $CH_2(OH)COO^-$, [Hbim] $CH_2(OH)COO^-$, respectively. But the precursor selenium powder has an absorption maximum of 431.96 nm with the transmittance 0.1364, as shown in Fig. 1.

By identifying the band gap energy of SeNPs, the optical properties of SeNPs were determined. From the absorption peaks, the optical energy band gap was calculated using the formula $E_g^0$ (eV) =12397.8/$\lambda_{max}$ (Å) [23] and compiled in Table 1. It is obvious that the calculated band gap values of the SeNPs were blue shifted from the precursor selenium. Increasing the band gap energies of SeNPs provides an indication of the quantum confinement effect due to the decreasing size of particles. Owing to the size effect, a wide increase in band gap of about 2.8196 eV was attained when compared with precursor selenium (2.8701 eV) [24].

**3. FT-IR Spectral Studies**

Fig. 2 shows the FT-IR spectrum of precursor selenium and SeNPs (FT-IR spectroscopy is effectively used to measure the particle formation [25]). In the case of precursor selenium the prominent absorption peaks were obtained at 3,434 $cm^{-1}$, 1,594 $cm^{-1}$, 1,384 $cm^{-1}$, 1,352 $cm^{-1}$, 765 $cm^{-1}$, whereas for SeNPs, absorption peaks were at 3,401 $cm^{-1}$, 1,584 $cm^{-1}$, 1,341 $cm^{-1}$, 761 $cm^{-1}$. Hence,

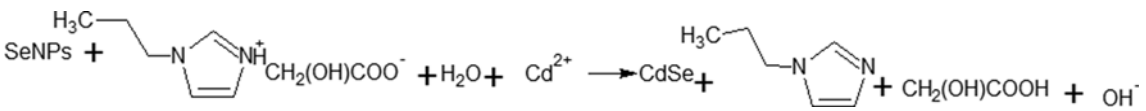


**Scheme 3. Schematic diagram of synthesis of CdSe nanoparticles.**

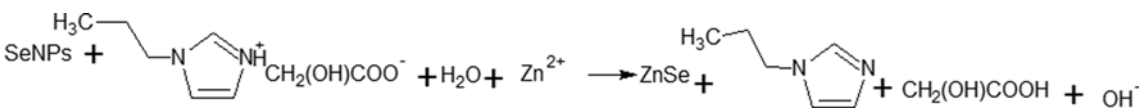


**Scheme 4. Schematic diagram of synthesis of ZnSe nanoparticles.**

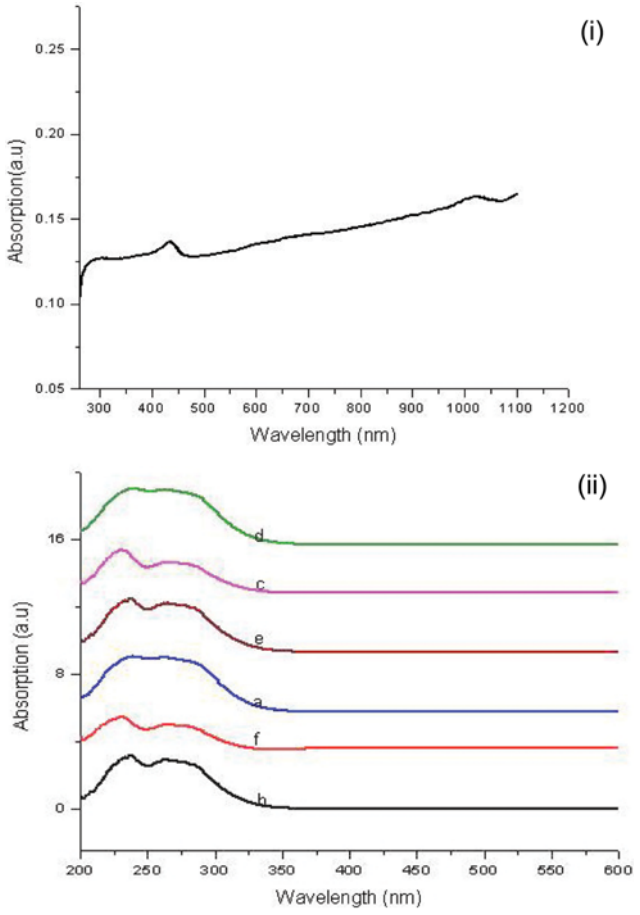


**Fig. 1. UV-absorption spectrum of precursors of (i) Se and (ii) SeNPs (Where a, b, c, d, e, f are the SeNPS synthesized from [Hmim]$CH_3CH(OH)COO^-$) [Heim]$CH_3CH(OH)COO^-$, [Hbim]$CH_3CH(OH)COO^-$, [Hmim]$CH_2(OH)COO^-$, [Heim] $CH_2(OH)COO^-$, [Hbim] $CH_2(OH)COO^-$ respectively).**

**Table 1. Band gap energies of SeNPs (Where a, b, c, d, e, f are the SeNPs synthesized from [Hmim]$CH_3CH(OH)COO^-$) [Heim]$CH_3CH(OH)COO^-$), [Hbim]$CH_3CH(OH)COO^-$), [Hmim]$CH_2(OH)COO^-$), [Heim] $CH_2(OH)COO^-$), [Hbim] $CH_2(OH)COO^-$) respectively)**

| S. No | Content | $\lambda$ max (Å) | Band gap (eV) |
|---|---|---|---|
| 1 | Precursor Se | 4319.6 | 2.8701 |
| 2 | a | 2629.0 | 4.7158 |
| 3 | b | 2239.0 | 5.5372 |
| 4 | c | 2179.0 | 5.6897 |
| 5 | d | 2594.7 | 4.7781 |
| 6 | e | 2218.0 | 5.5896 |
| 7 | f | 2136.9 | 5.8018 |

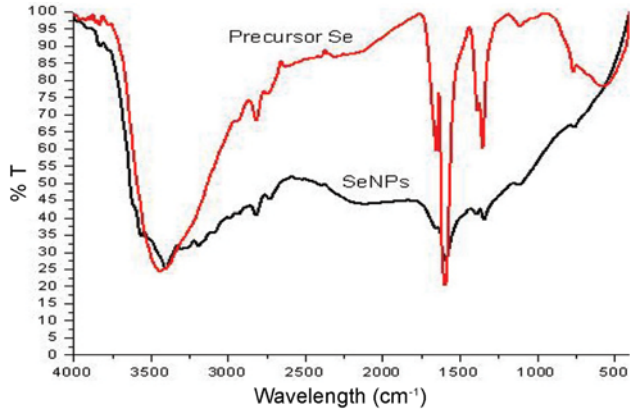


**Fig. 2. FT-IR spectrum of precursors of Se and SeNPs.**

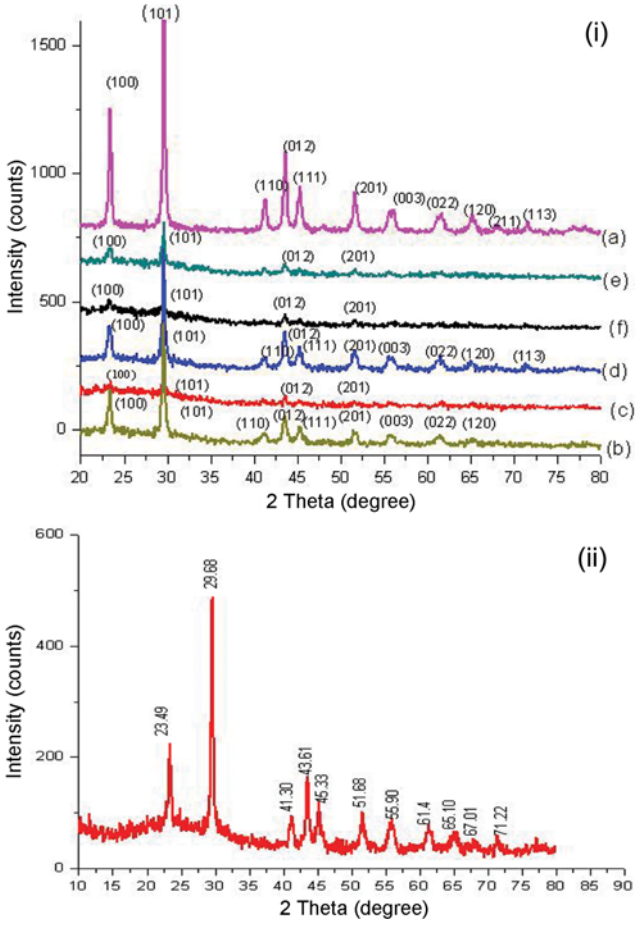


**Fig. 3. XRD pattern of precursors of selenium (i) and (ii) SeNPs (Where a, b, c, d, e and f are the SeNPs synthesized from [Hmim]$CH_3CH(OH)COO^-$, [Heim]$CH_3CH(OH)COO^-$, [Hbim]$CH_3CH(OH)COO^-$, [Hmim]$CH_2(OH)COO^-$, [Heim] $CH_2(OH)COO^-$, [Hbim] $CH_2(OH)COO^-$ respectively).**

the FT-IR spectrum of SeNPs differs considerably from the precursor selenium in a bulk form. This distinguishing feature exhibited by SeNPs is termed to the fact that, in the case of SeNPs the surface to volume ratio is noted to be very high when compared to precursor selenium in a bulk form. Moreover, Fig. 2 makes evident that the width and intensity of peaks in FT-IR spectrum were influenced more by the particle size. The peaks of SeNPs had smaller intensity (smaller the percent transmittance) and narrow width, whereas the peaks of precursor selenium have higher intensity (higher the percent transmittance) and broader width. Thus, the size of the particle decreases with an increase in the width of

**Table 2. XRD pattern of SeNPs (Where a, b, c, d, e, f are the SeNPs synthesized from [Hmim]$CH_3CH(OH)COO^-$, [Heim]$CH_3CH(OH)COO^-$, [Hbim]$CH_3CH(OH)COO^-$, [Hmim]$CH_2(OH)COO^-$, [Heim] $CH_2(OH)COO^-$, [Hbim] $CH_2(OH)COO^-$ respectively)**

| S. No. | Content | 2$\theta$ | hkl Planes | Average size (nm) |
|---|---|---|---|---|
| 1 | a | 23.39, 29.59, 41.22, 43.56, 45.25, 51.59, 55.55, 61.4, 65.08, 67.9, 71.2 | (100), (101), (110), (012), (111), (201), (003), (022), (120), (211), (113) | 24.2050 |
| 2 | b | 23.36, 29.55, 41.2, 43.52, 45.24, 51.6, 55.7, 61.3, 65.1 | (100), (101), (110), (012), (111), (201), (003), (022), (120) | 23.9569 |
| 3 | c | 23.36, 29.55, 43.55, 51.59 | (100), (101), (012), (201) | 20.4583 |
| 4 | d | 23.33, 29.56, 41.14, 43.51, 45.17, 51.55, 55.77, 61.32, 65.11, 71.19 | (100), (101), (110), (012), (111), (201) (003), (022), (120), (113) | 23.6071 |
| 5 | e | 23.2, 29.57, 43.55, 52.2 | (100), (101), (012), (201) | 22.4732 |
| 6 | f | 23.31, 29.53, 43.51, 51.58 | (100), (101), (012), (201) | 19.4439 |

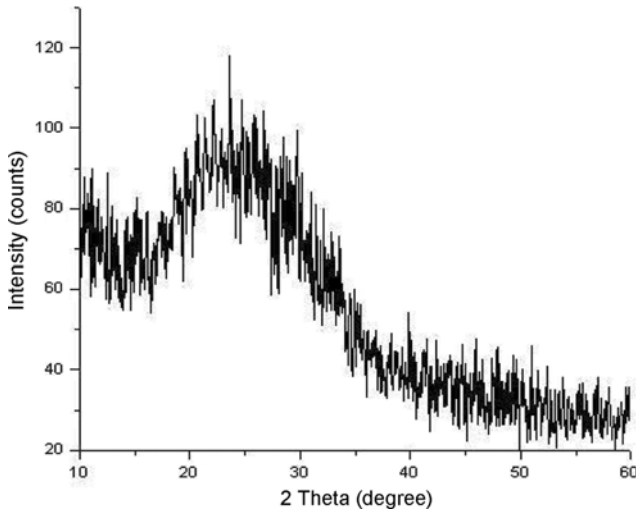


**Fig. 4. XRD pattern of CdSe nanoparticles.**

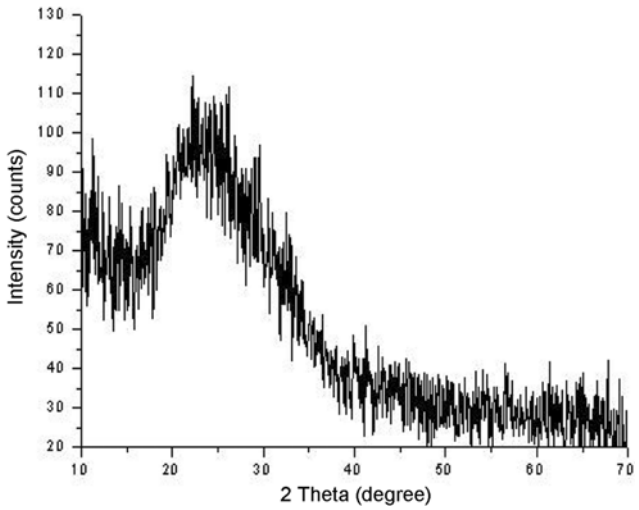


**Fig. 5. XRD pattern of ZnSe nanoparticles.**

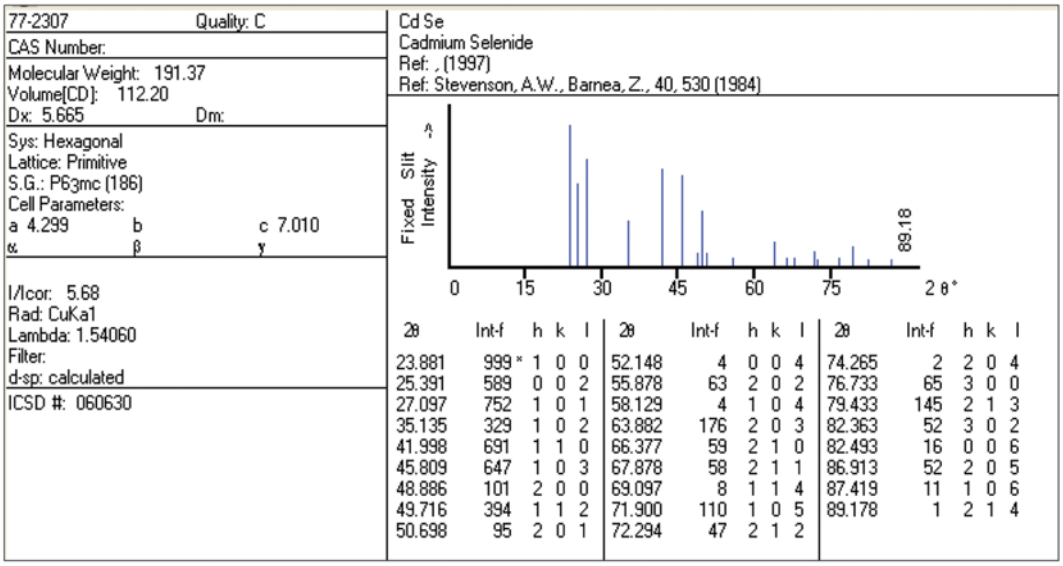


**Fig. 6. JCPDS card number (77-2307) of CdSe sample.**

the peaks and decrease in the intensity. Thereby, the formation of SeNPs was confirmed by FT-IR analysis.

**4. X-ray Diffraction Analysis**

The XRD pattern of the synthesized SeNPs matches well with

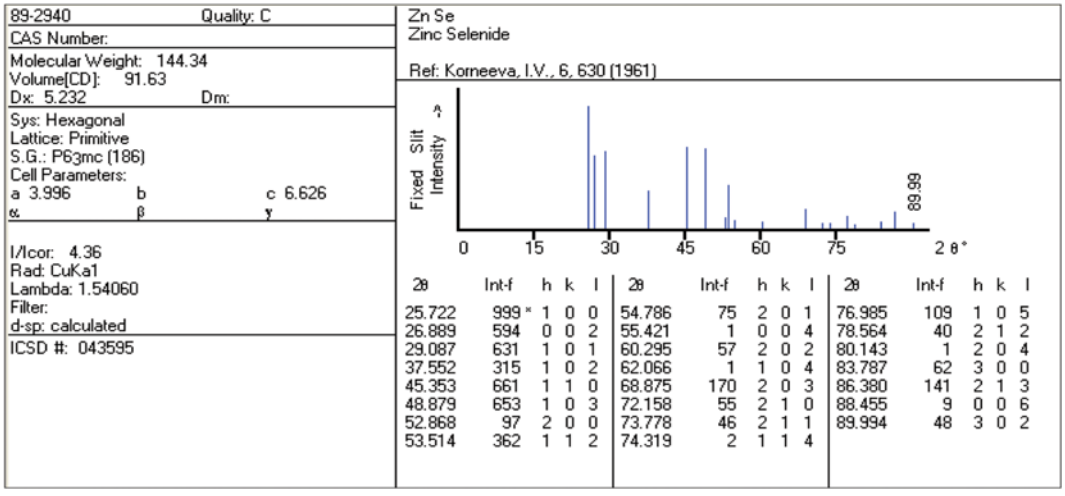


**Fig. 7. JCPDS card number (89-2940) of ZnSe sample.**

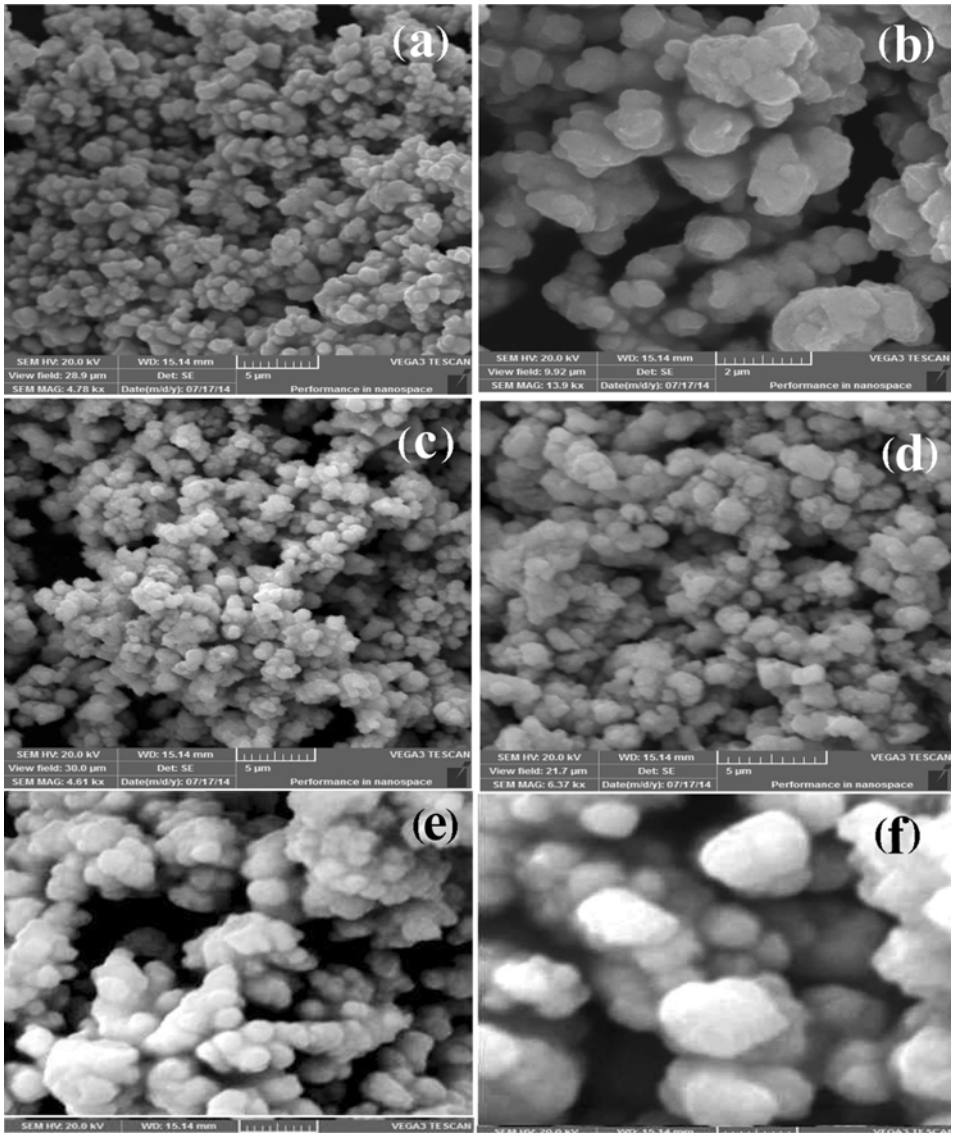


**Fig. 8. SEM images of SeNPs (Where figures a, b, c, d, e and f are the SeNPs synthesized from [Hmim]$CH_3CH(OH)COO^-$, [Heim]$CH_3CH(OH)COO^-$, [Hbim]$CH_3CH(OH)COO^-$, [Hmim]$CH_2(OH)COO^-$, [Heim] $CH_2(OH)COO^-$, [Hbim] $CH_2(OH)COO^-$) respectively).**

the standard Se powder JCPDS Card No. 86-2246 as shown in Fig. 3(i) and (ii) confirming the formation of SeNPs. The SeNPs containing hexagonal structure with lattice constants (a=4.4245 Å, c=5.0520 Å) were well in agreement with the literature values (a= 4.368 Å, c=4.958 Å). The average sizes of SeNPs using different PILs were calculated using Debye-Scherrer equation and compiled in Table 2. The SeNPs synthesized from [Hbim] $CH_3CH(OH)COO^-$), [Hbim] $CH_2(OH)COO^-$) were found to be smaller (20.4583 nm and 19.4439 nm, respectively) when compared to other SeNPs obtained from the rest of the PILs. Evident by the fact that increased alkyl chain in imidazolium cation stabilized the SeNPs strongly, resulting in smaller particles. Thus, PILs acts also as a stabilizer, which predominantly resulted in smaller nanoparticles. The smaller nanoparticles were acquired in more pre-organized ionic liquid structure.

The XRD pattern of the synthesized CdSe is shown in Fig. 4. The XRD measurement of CdSe revealed that the position of the diffracted peak matches well with the standard powder diffraction data (a=4.299 Å, c=7.010 Å). Various peaks of CdSe 23.80, 25.21, 27.81, 44.91, 62.6° were obtained due to diffraction from (100), (002), (001), (103), (203) planes of hexagonal CdSe which were in a better agreement with hexagonal structure JCPDS Card No. 77-2307 (Fig. 5). From the different $\theta$ values, the calculated average particle size was observed to be about 29.97 nm.

XRD measurements of ZnSe (Fig. 6) made clear that the position of the diffracted peak matches well with the standard powder diffraction data (a=3.996 Å, c=6.626 Å). Several peaks of ZnSe 25.69, 26.17, 30.12, 36.9, 45.21° were acquired due to diffraction from (100), (002), (101), (102), (110) planes of hexagonal ZnSe, which agrees well with hexagonal structure JCPDS Card No. 89-2940 (Fig. 7). From the different $\theta$ values, the calculated average particle size was noted to be about 22.73 nm.

**5. Scanning Electron Microscope (SEM) Analysis**

The SEM analysis of SeNPs revealed that all the synthesized SeNPs are spherical (Fig. 8). It is evident from the SEM images of CdSe and ZnSe (Figs. 9 and 10, respectively) that CdSe and ZnSe had pebble- and cluster-like structure, respectively.

The EDX analysis confirmed that the SeNPs contained pure selenium without elemental impurities (Fig. 11). In addition, the chemical composition of CdSe and ZnSe was also confirmed by EDX analysis, as shown in Figs. 12 and 13, respectively.

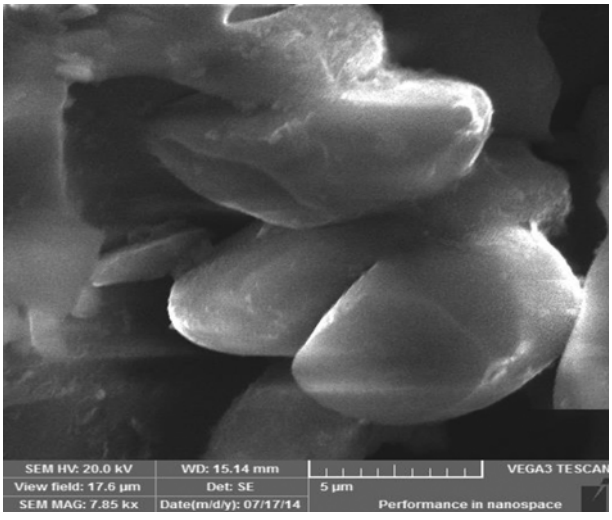


**Fig. 9. SEM image of CdSe nanoparticles.**

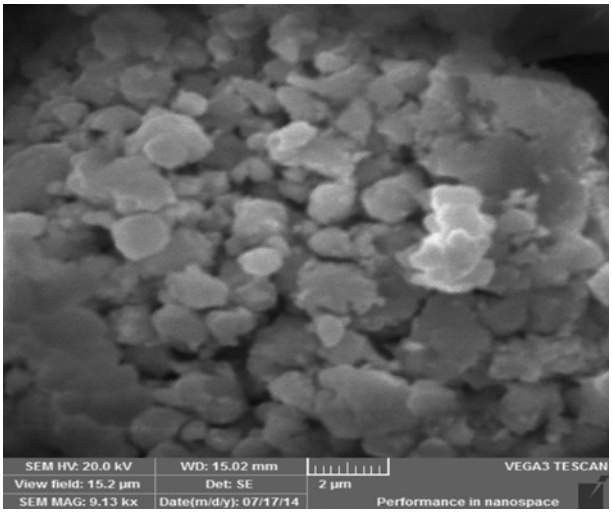


**Fig. 10. SEM image of ZnSe nanoparticles.**

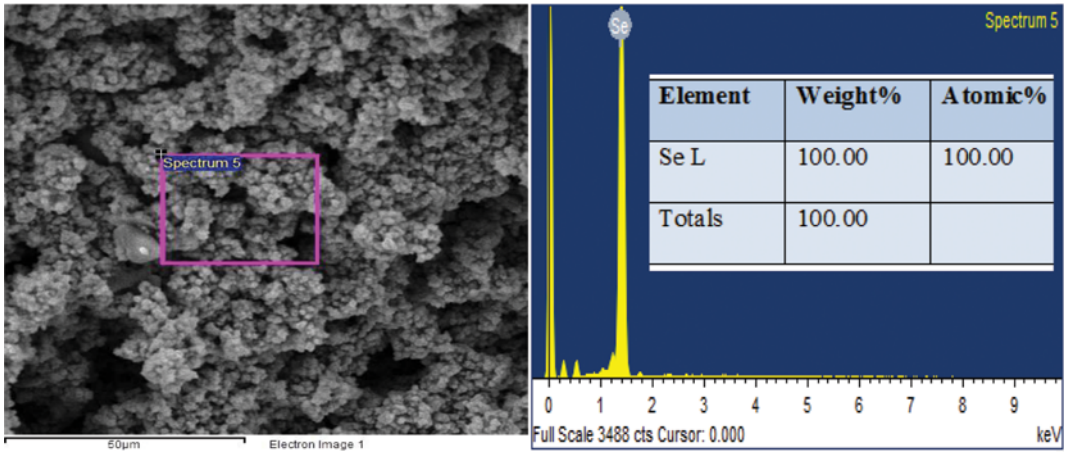


**Fig. 11. EDX analyses of SeNPs.**

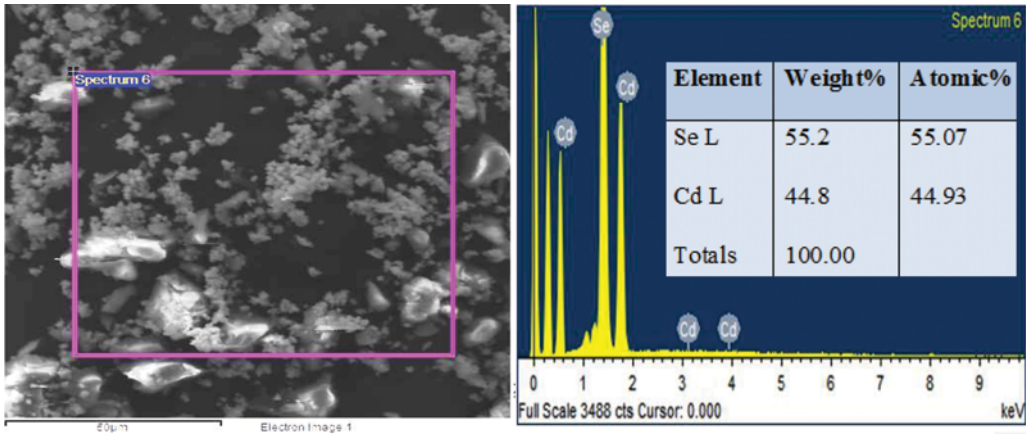


**Fig. 12. EDX analysis of CdSe nanoparticles.**

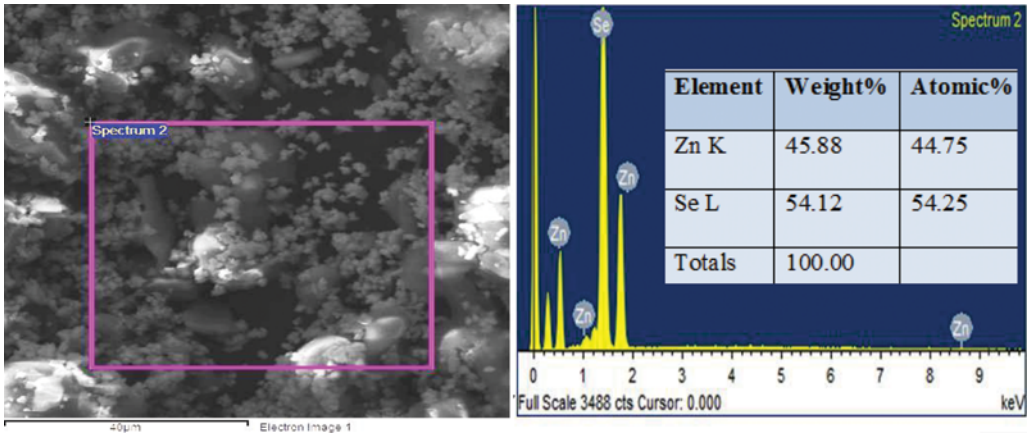


**Fig. 13. EDX analysis of ZnSe nanoparticles.**

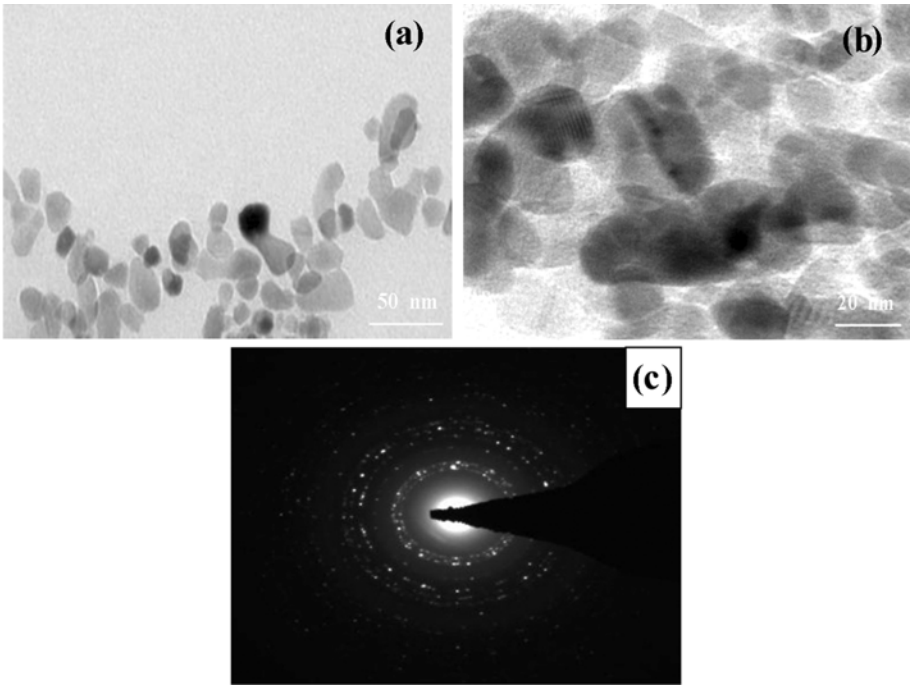


**Fig. 14. HR-TEM images (a), (b) and SAED pattern (c) of SeNPs.**

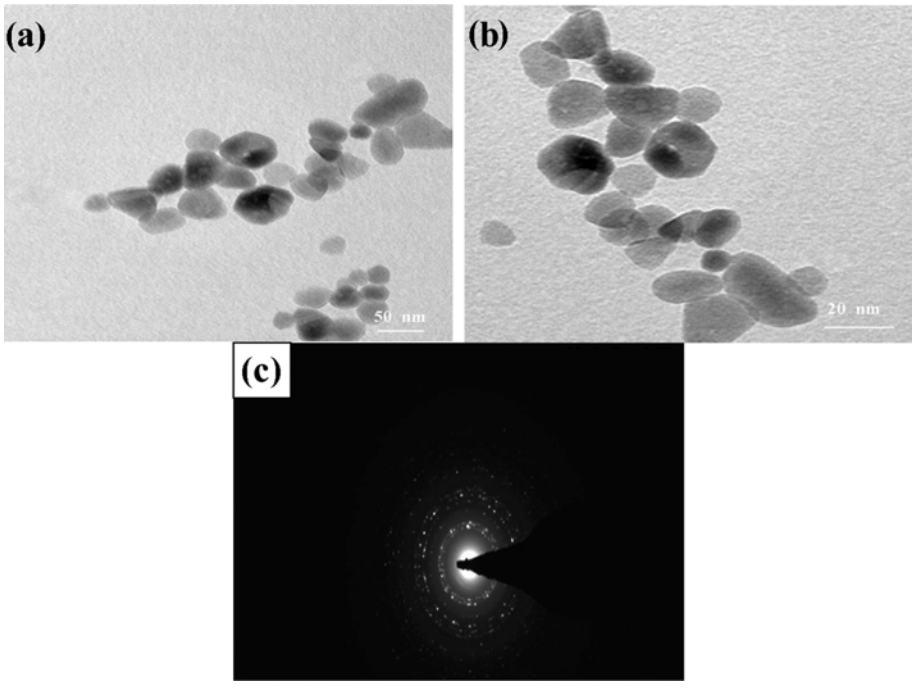


**Fig. 15. HR-TEM images (a), (b) and SAED pattern (c) of CdSe nanoparticles.**

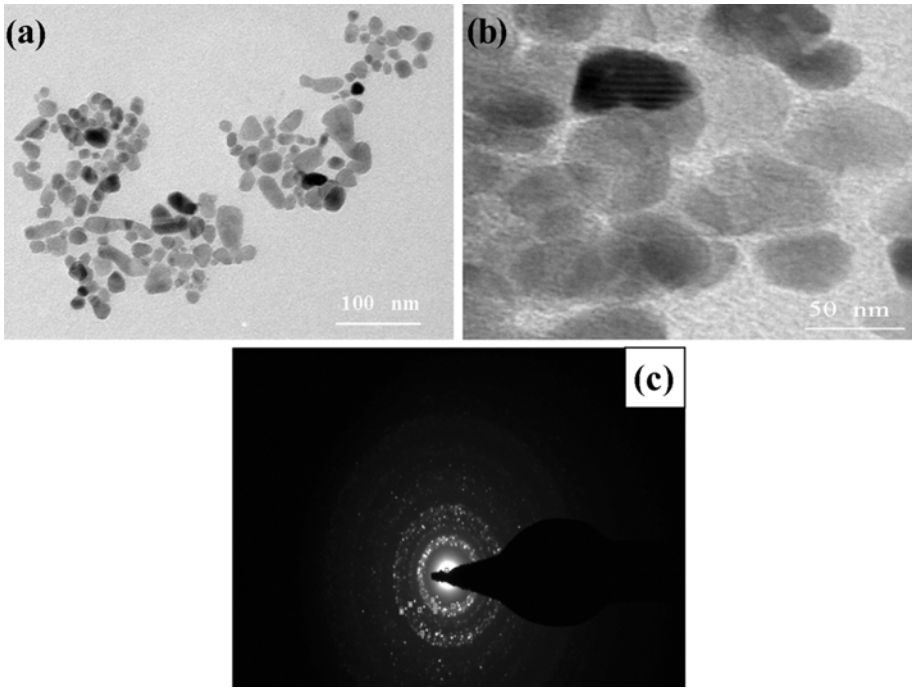


**Fig. 16. HR-TEM images (a), (b) and SAED pattern (c) of ZnSe nanoparticles.**

**6. Transmission Electron Microscope (TEM) Analysis**

High resolution transmission electron microscope (HR-TEM) analysis provides actual size, shape and surface topography of the nanoparticles. A typical TEM image of SeNPs is shown in Figs. 14(a) and (b). The spherical shape of the particles visible in the TEM image show a size distribution around 20 nm. In addition, the TEM images of CdSe (Fig. 15(a) and (b)), ZnSe (Fig. 16(a) and (b)) confirm their pebble and cluster morphology, respectively. Fig. 14(c), 15(c) and 16(c) show the selected area electron diffraction (SAED) patterns of SeNPs, CdSe and ZnSe, respectively. The SAED patterns confirm the single crystal nature of the nanoparticles.

**7. Thermogravimetric Analysis (TGA) and Differential Thermal Analysis (DTA)**

The thermal analysis (TGA) of SeNPs proved stability and it

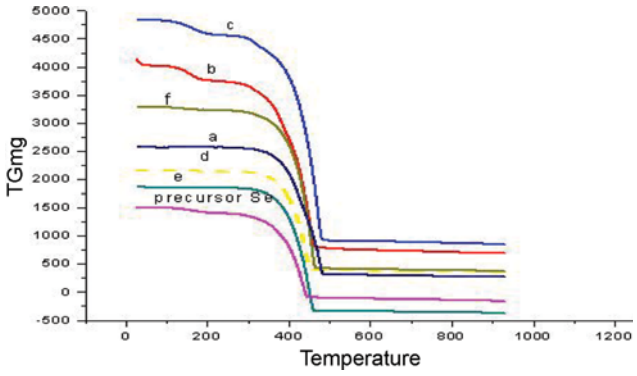


**Fig. 17. TGA analysis of SeNPs (Where a, b, c, d, e and f are the SeNPs synthesized from [Hmim]$CH_3CH(OH)COO^-$, [Heim] $CH_3CH(OH)COO^-$, [Hbim]$CH_3CH(OH)COO^-$, [Hmim] $CH_2(OH)COO^-$, [Heim] $CH_2(OH)COO^-$, [Hbim] $CH_2(OH)COO^-$ respectively).**

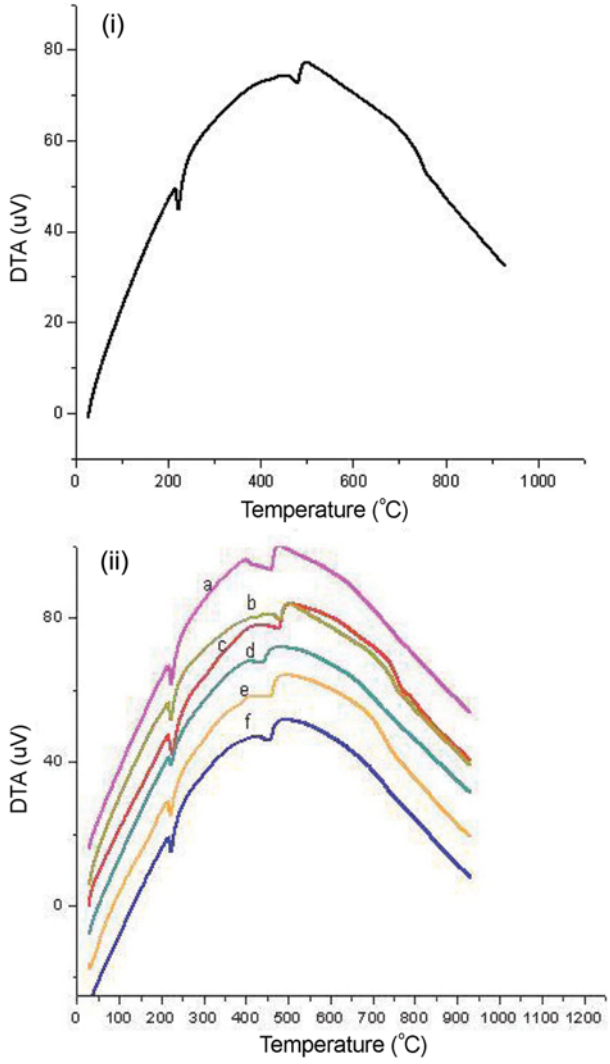


**Fig. 18. DTA analysis of precursor (i) selenium and (ii) SeNPs (Where a, b, c, d, e and f are the SeNPs synthesized from [Hmim] $CH_3CH(OH)COO^-$, [Heim]$CH_3CH(OH)COO^-$, [Hbim] $CH_3CH(OH)COO^-$, [Hmim]$CH_2(OH)COO^-$, [Heim] $CH_2(OH)COO^-$, [Hbim] $CH_2(OH)COO^-$ respectively).**

started to decompose between 260-330 °C whereas the initial selenium precursor at 240 °C (Fig. 17). Thus the SeNPs have higher thermal stability. SeNPs synthesized using [Hbim] $CH_2(OH)COO^-$ were strongly stabilized, having a very high thermal decomposition temperature of 330 °C, thereby attaining higher thermal stability (Fig. 14).

From the DTA measurement it is obvious that the melting point of SeNPs lies between 218-220 °C (Fig. 18), while precursor selenium had 222.2 °C. The melting point of solid materials can be reduced to a higher extent when processed as nanostructures [26]. As a result of lower particle size, the SeNPs synthesized by [Hbim] $CH_2(OH)COO^-$) acquired a low melting point at about 218 °C.

## CONCLUSIONS

SeNPs were synthesized successfully using six different imidazolium protic ionic liquids. The XRD measurements and TEM analysis confirm that the sizes of synthesized SeNPs were in a range of 19-24 nm. The morphology of the SeNPs was identified by means of SEM and TEM analysis which revealed that the SeNPs were spherical. The EDX analysis of SeNPs confirmed the presence of elemental selenium without any impurities. Furthermore, the synthesized SeNPs had an increased optical energy band gap and were blue shifted from the initial selenium precursor. Thus, SeNPs provided a scope of optical applications. The thermal stability of the SeNPs could be confirmed by TGA measurements, and the synthesized SeNPs have a low melting point around 218 °C. The chalcogenide nanomaterials like CdSe and ZnSe with a particle size of 29.97 nm and 22.73 nm, respectively, were synthesized by SeNP obtained from [Hbim] $CH_2(OH)COO^-$) as a precursor. The morphology of CdSe and ZnSe was confirmed by SEM, TEM analysis, and the elemental composition was confirmed by their EDX analysis. Hence the synthesized SeNPs may serve as a template to generate important nanomaterials.

## REFERENCES

1. K. S. Kim, N. D. Demberelnyamba, S. W. Yeon, S. Choi, J. H. Cha and H. Lee, *Korean J. Chem. Eng.*, **22**, 717 (2005).
2. J. E. Kim, J. W. Kang and J. S. Lim, *Korean J. Chem. Eng.*, **32**, 1678 (2015).
3. Y. H. Moon, S. M. Lee, S. H. Ha and Y. M. Koo, *Korean J. Chem. Eng.*, **23**, 247 (2006).
4. J. H. Cha, K. S. Kim, S. Choi, S. H. Yeon, H. Lee, C. S. Lee and J. J. Shim, *Korean J. Chem. Eng.*, **24**, 1089 (2007).
5. M. Antonietti, D. B. Kuang, B. Smarsly and Z. Yong, *Angew. Chem.*, **43**, 4988 (2004).
6. W. H. Suh, Y. H. Suh and G. D. Stucky, *Nano Today*, **4**, 27 (2009).
7. J. A. Dahl, B. L. S. Maddux and J. E. Hutchison, *Chem. Rev.*, **107**, 2228 (2007).
8. J. Dupont, G. S. Fonseca, A. P. Umpierre, P. F. P. Fichtner and S. R. Teixeira, *J. Am. Chem. Soc.*, **124**, 4228 (2002).
9. Z. Li, Y. Luan, T. Mu and G. Chen, *Chem. Commun.*, **10**, 1258 (2009).
10. F. Endres, M. Bukowski, R. Hempelmann and H. Natter, *Angew. Chem. Int. Ed.*, **42**, 3428 (2003).

11. S. Shafiu, B. Unal and A. Baykal, *J. Inorg. Organomet. Polym.*, **23**, 1335 (2013).
12. A. Baykal, M. Gunay, M. S. Toprak and H. Sozeri, *Mater. Res. Bull.*, **48**, 378 (2013).
13. A. Jagminas, I. Gailiute, G. Niaura and R. Giraitis, *Chemija.*, **16**, 15 (2005).
14. X. Cao, Y. Xie, S. Zhang and F. Li, *Adv. Mater.*, **16**, 649 (2004).
15. J. Zhang, H. Wang, X. Yan and L. Zhang, *Life Sci.*, **76**, 1099 (2005).
16. B. Gates, B. Mayers, B. Cattle and Y. N. Xia, *Adv. Funct. Mater.*, **12**, 219 (2002).
17. T. W. Smith and R. A. Cheatham, *Macromolecules*, **13**, 1203 (1980).
18. D. H. Son, S. M. Hughes, Y. Yin and A. P. Alivisatos, *Science*, **306**, 1009 (2004).
19. P. H. C. Camargo, Y. H. Lee, U. Jeong, Z. Zhou and Y. Xia, *Langmuir*, **23**, 2985 (2007).
20. B. Langi, C. Shah, K. Singh, A. Chaskar, M. Kumar and P. N. Balaji, *Mater. Res. Bull.*, **45**, 668 (2010).
21. B. Meenatchi and V. Renuga, *Int. J. Adv. Res.*, **2**, 1107 (2014).
22. M. Antonietti, D. Kuang, B. Smarsly and Y. Zhou, *Angew. Chem. Int. Ed.*, **43**, 4988 (2004).
23. S. M. Sze, Physics of semiconductor devices (2nd Ed.), Wiley, Delhi (1981).
24. B. Ludolph and M. A. Malik, *Chem. Commun.*, **17**, 1849 (1998).
25. J. A. Eastman, L. J. Thompson and B. J. Kestel, *Phys. Rev. B*, **48**, 84 (1993).
26. A. R. Ingole, S. R. Thakare, N. T. Khati, A. V. Wankhade and D. K. Burghate, *Chalcogenide Lett.*, **7**, 485 (2010).